Title: "Centrosome Amplification promotes cell invasion via cell-cell contact disruption and Rap-1 activation"

Authors: Anu Prakash[1], Shishir Paunikar[1], Mark Webber[1], Emma McDermott[2], Sri H. Vellanki[6], Kerry Thompson[2], Peter Dockery[2], Hanne Jahns[3], James A.L. Brown[4,5], Ann M. Hopkins[6], Emer Bourke.[1Φ*]

Affiliations:
[1] Lambe Institute for Translational Research, Discipline of Pathology, Centre for Chromosome Biology, National University of Ireland, Galway; [2]Centre for Microscopy and Imaging, Discipline of Anatomy, School of Medicine, NUIG; [3]Pathobiology Section, School of Veterinary Medicine, University College Dublin; [4]Department of Biological Sciences, University of Limerick; [5]Limerick Digital Cancer Research Centre (LDCRC) and Health Research Institute, University of Limerick; [6]Department of Surgery, Beaumont Hospital, Royal College of Surgeons in Ireland.

Φ ORCID: 0000-0002-2218-3114

* Author to whom correspondence should be addressed: emer.bourke@nuigalway.ie

Author Contributions: AP and EB designed, and planned manuscript and AP and SP performed all experiments. EMD and MW contributed to sample processing and data analysis. KT and PD provided advice on data interpretation and analysis. HJ contributed to in vivo histological analysis through specialised expertise in veterinary histopathology. JB advised on experimental conception, data analysis and manuscript editing. AMH and SHV advised on experimental conception. EB and AP manuscript writing and EB final approval of manuscript. All authors provided critical feedback and helped shape the final manuscript.

Key words: centrosome amplification, invasion, metastases, breast cancer.

Abbreviations: Centrosome amplification (CA), Chicken Chorioallantoic membrane (CAM), microtubule organising centre (MTOC), ninein-like protein (NLP), human umbilical vein endothelial cells (HUVEC), CA-induced (CA+), Doxycycline (DOX), Immunofluorescence (IF).

Statement: Centrosome amplification alone drives early tumourigenic change in normal breast epithelial cells

ABSTRACT

Centrosome amplification (CA), a prominent feature of human cancers linked to genomic instability and tumourigenesis *in vivo*, is observed as early as pre-malignant metaplasia, increasing with progression from dysplasia to neoplasia. However, the mechanistic contributions of CA to tumourigenesis are not fully understood.

Using non-tumourigenic breast cells (MCF10A), we demonstrate that induction of CA (by CDK1 inhibition or PLK4 overexpression) increased both the migration and invasion of non-tumourigenic cells. Mechanistically, we found small GTPase Rap-1 was activated upon CA induction. Rap-1 inhibition (using GGTI-298) blocked CA-induced migration, invasion and ECM attachment, demonstrating the role of Rap-1 in CA induced tumourigenesis.

Induction of CA in a long-term cell culture system disrupted epithelial cell-cell junction integrity, via dysregulation of expression and subcellular localisation of cell junction proteins (ZO-1, Occludin, JAM-A & β-catenin). Physically, CA inhibited apical junctional complex formation, visualised by transmission electron microscopy. Furthermore, CA induction in non-tumourigenic cells elevated β-integrin 3 expression, potentially mediating increased cell attachment to the extracellular matrix (ECM) induced by CA. Simultaneously, CA induced elevated expression of matrix metalloprotease MMP1 and MMP13 facilitating ECM degradation and cell invasion.

In vivo validation in a Chicken Embryo xenograft model, showed CA+ MCF10A cells invaded into the chicken mesodermal layer, characterised by inflammatory cell infiltration and a marked focal reaction between chorioallantoic membrane and cell graft. This reaction was inhibited by pre-treatment of CA+ MCF10A cells with Rap-1 inhibitor GGTI-298. Inhibition of CA in metastatic breast cancer cells with high levels of endogenous CA (triple negative cell line MDA-MB-231), using PLK4 inhibitor Centrinone B, abrogated their metastatic capacity *in vitro*.

Here, we demonstrated CA induction in normal cells confers early tumourigenic changes which promote tumour progression, mediated by ECM disruption, altered cell-cell contacts, and Rap-1-dependent signaling. These insights fundamentally demonstrate the mechanism of how CA induces tumourigenesis in normal cells, alone and without requiring additional pre-tumourigenic alterations.

INTRODUCTION

Centrosomes play essential roles in averting genomic instability by regulating cell cycle control, spindle assembly and ultimately cell replication. Centrosome amplification (CA), a numerical centrosomal defect (≥3 centrosomes per cell) is a hallmark feature of many high-grade human tumours (Chan, 2011). CA is triggered by well-characterised mechanisms including cytokinesis failure, dysregulation of centrosome duplication proteins and pericentriolar material (PCM) fragmentation (reviewed in (Godinho *et al*, 2014)). Furthermore, extra centrosomes are directly induced *in vitro* by DNA damage and defects in DNA repair pathways linking their presence to inherent genetic instability of tumour cells (Bourke *et al*, 2010; Bourke *et al*, 2007; Dodson *et al*, 2004). However, it is increasingly clear that aberrant centrosome numbers are not necessarily a downstream consequence of tumorigenesis and centrosome abnormalities directly perpetuate genomic instability by promoting chromosome missegregation (Cosenza & Kramer, 2016; Ganem *et al*, 2009) and cellular invasion via cell-autonomous and non-autonomous mechanisms (Adams *et al*, 2021; Arnandis *et al*, 2018). CA induction promotes tumourigenesis *in vivo* (Coelho *et al*, 2015; Levine *et al*, 2017; Sercin *et al*, 2016) and has been observed as early as pre-malignant metaplasia, increasing during progression to dysplasia, accompanied by p53 mutation and loss (Lopes *et al*, 2018; Pihan *et al*, 2003; Segat *et al*, 2010). Together, this evidence suggests that CA plays a crucial role in early tumour initiation and malignant progression.

In its capacity as the major microtubule organising centre (MTOC), the centrosome orchestrates microtubule (MT) assembly pending mitosis whilst also controlling cell positioning, polarity and motility through its links to the acto-myosin cytoskeleton, cell-cell and cell-extracellular matrix (ECM) junctions (Bettencourt-Dias, 2013; Bornens, 2012). Cell-cell attachments are key to maintaining barrier function in polarised epithelia, and are mediated by highly specialised junctional complexes consisting of tight junctions, adherens junctions, desmosomes and gap junctions (Garcia *et al*, 2018). Crucially, the formation and regulation of these junctions is dependent on their interactions with cytoskeletal polymers of microtubules and actin, both of which nucleate from the centrosome (Farina *et al*, 2016; Vasileva & Citi, 2018). It is therefore logical that abnormalities of the centrosome, structural or numerical, may impact significantly on cell-cell junction function, promoting cell detachment from the epithelial layer. Indeed, recent studies have shown that structural centrosome anomalies induced by ninein-like protein (NLP) overexpression in MCF10A breast epithelia, disrupt epithelial polarity and cell-cell contacts via dysregulation of E-cadherin localisation within adherens junctions mediated by small GTPase Rac1 and Arp2/3 signalling (Ganier *et al*, 2018). This leads to increased cell stiffness, detachment from the epithelium and cell budding towards the extracellular matrix. CA induced by PLK4 overexpression in MCF10A cells, generates increased MT nucleation and polymerisation, also causing Rac1 activation and Arp2/3-dependent actin polymerisation, leading to invasive lamelipodia formation in 3D cultures. The invasive phenotype is accompanied by loss of cell-cell adhesion, disruption of junction size and positioning as well as dysregulation of E-cadherin junctional localization (Godinho *et al.*, 2014). In human umbilical vein endothelial cells (HUVEC), induction of CA alters cell polarity and perturbs luminogenesis of newly formed endothelial sprouts accompanied

by chaotic localization of vascular endothelial (VE)-cadherin, resulting in the disruption of adherens junction stability (Buglak *et al*, 2020). All evidence points to perturbations of cell-cell and cell-ECM contacts underlying the CA-induced metastatic phenotype via epithelial layer detachment, but this remains to be explored in detail.

Another central step towards local invasion of tumour cells into adjacent tissue is the degradation of ECM components via matrix metalloproteinase (MMP) secretion (Kessenbrock *et al*, 2010). This family of zinc-dependent endopeptidases are involved in physiological tissue remodelling as well as pathological ECM breakdown within the tumour microenvironment. Emerging evidence of the role of CA in cell migration and invasion points to a possible link between CA and increased MMP expression. Tumours derived from the injection of tetraploid cells into mice are associated with high levels of centrosome amplification accompanied by amplification of an MMP gene cluster (Fujiwara *et al*, 2005). Furthermore, treatment with the broad spectrum matrix metalloprotease (MMP) inhibitor, marimastat (BB-2516), decreased the fraction of CA-induced invasive acini in MCF10A 3D cultures (Godinho *et al.*, 2014). Proposed intracellular mediators of CA-induced effects include the subfamilies of small GTPases, Rho and Ras, which play roles as molecular switches integrating signals from the membrane to actin-cytoskeletal changes to a wide range of effector proteins of migration and invasion, including the expression of MMPs (Sahai *et al*, 2001). It has been shown that the Rho-GTPase Rac1 is activated by the induction of CA breast epithelial cells and that a Rac1 inhibitor (NSC23766) partially rescued the invasive phenotype induced by CA (Godinho *et al.*, 2014). The downstream mediation of CA-induced cellular invasion of the ECM is complex and multifaceted, requiring further detailed characterisation.

In this study, we investigate how CA induction alone (in non-tumourigenic cells) can drive the initial stages of tumourigenesis by promoting cell invasiveness (in both non-tumourigenic and tumourigenic breast epithelial cells) via alteration of extracellular contacts (cell-cell and cell-ECM) and dysregulated MMP/TIMP production, mediated through Rap1 signalling. The results are validated using in our semi-3D long-term cell culture system and an *in vivo* (chick embryo xenograft) model where implantation of CA-induced (CA+) MCF10A cells results in cell invasion into the chorioallantoic membrane and a vigorous proliferative focal reaction involving immune cell infiltration.

RESULTS

Centrosome Amplification increases cellular migration and invasion *in vitro* and *in ovo* chick embryo xenograft model.

Polo-like kinase (PLK4) is the master regulator kinase of the centrosome duplication cycle (Bettencourt-Dias *et al*, 2005; Habedanck *et al*, 2005). Non-tumourigenic breast epithelial MCF10A PLK4 cell lines employed in the current study were engineered with doxycycline(Dox)-inducible PLK4 transgenes; Dox-induced Wild Type gene PLK4 expression induces CA (CA+ MCF10A) and a truncated PLK4 variant (PLK4 608; amino acids 1–608 of PLK4), which lacks the C-terminal centrosome localization domain and does not induce CA when overexpressed (Godinho *et al.*, 2014). Dox treatment led to a significant ($p=0.02$) CA induction in 80% (±1.26 sem) of cells MCF10A PLK4 population after 48h (Fig. 1A-B). We measured cell invasion and migration post-CA induction using Matrigel-coated and uncoated transwell assays respectively. CA+ MCF10A PLK4 cells had a significant ($p<0.05$) ~3-fold increase in invasion (Fig. 1C), and a significant ($p<0.02$) ~2-fold increase in migration (Fig. 1D), compared to both untreated controls or PLK4 608. To independently validate that these findings are dependent on CA-induction, we induced CA in WT MCF10A by CDK1 inhibition, as previously demonstrated (Bourke *et al.*, 2010), using the CDK1 pharmacological inhibitor RO3306 (Steere *et al*, 2011). RO3306 treatment significantly induced CA ($p=0.2$), migration and invasion ($p<0.05$) (Fig. S1A-C).

To investigate how CA induction could initiate early tumourigenic change *in vivo*, we employed a chicken embryo xenograft model. The chicken chorioallantoic membrane (onto which the MCF10A are grafted) consists of the chorionic epithelium (the outer layer) with a superficial vascular plexus, and the intermediate mesoderm layer and the allantoic epithelium (inner layer). CA+ MCF10A PLK4 were implanted (embedded in matrigel) on the chorioallantoic membrane for 5 days, allowing extremely early changes to be characterised in detail (not previously explored using *in vivo* mouse models (Coelho *et al.*, 2015; Levine *et al.*, 2017; Sercin *et al.*, 2016)). Histological evaluation CA+ MCF10A PLK4 invaded into the chorionic epithelium (at the cell-matrigel interface) (black arrows, Fig. 1E) with a multifocal moderate to marked reaction of the CE with proliferation of mesodermal cells (red arrows, Fig. 1E), multifocal heterophil infiltration and dilated lymphatics in the intermediate mesoderm layer (green arrows, Fig. 1E). CA resulted in invasion of MCF10A cells (anti-human Cytokeratin 5 positive) into the chicken tissue, forming epithelial cell nests within the intermediate chicken mesodermal layer (Fig. 1E dotted circles and enlarged panel). Interestingly, the histology analysis also indicated that CA+ MCF10A sections displayed clear secondary tumour characteristics including haemorrhaging, necrosis and calcification at the CAM/matrigel interface (Fig. S2 A-B). Together these results show that CA induction alone in non-tumourigenic cells is sufficient to induce a migratory and invasive cellular phenotype (*in vitro* and *in vivo*), and induction of secondary tumour-associated changes in the surrounding tissue *in vivo*.

To evaluate the contribution of CA to an invasive phenotype, we utilized MDA-MB-231 (triple negative breast cancer; TNBC) cells with endogenously high CA levels. CA was blocked using the PLK4 specific inhibitor Centrinone B. Centrinone B has been previously reported to reduce centrosome and centriole numbers, with (<48 hours) treatment reverting CA lines to a normal centrosome complement (1-2 centrosomes) and >48 hours treatment leading to complete centrosome depletion (Denu *et al*, 2020; Denu *et al*, 2018; Marteil *et al*, 2018; Wong *et al*, 2015). Cancer cell lines treated with Centrinone B for less than 48h reverted to a normal centrosome complement of 1-2 centrosomes whereas longer treatment lead to complete centrosome depletion (Wong *et al.*, 2015). Centrinone B treated MDA-MB-231 had significantly ($p<0.05$) reduced %CA from 39.75 ± 4.6% to 10.25 ± 0.35% (data not shown), Centrinone B treated MDA-MB-231 cells showed significantly ($p=0.001$) reduced invasion (2.5-fold), and significantly ($p<0.05$) reduced migration (2.7-fold) (Fig. 1F-G).

To confirm that Centrinone B does not affect migration or invasion independently of high CA levels, MDA-MB-468 cells (a second invasive TNBC cell line) with low endogenous levels of CA (5-10% cells) (data not shown) were also tested. Centrinone B treatment of MDA-MB-468 cells did not significantly reduce the number of cells which migrated or invaded across the membrane (reduction of 3% and 16% respectively; Fig. S1D). This suggests that in cancer cells with high CA, the increased migration and invasion is dependent on increased CA. However, in cancer cells with low CA, the increased migration and invasion is independent of CA.

Centrosome Amplification induced migration and invasion involves activation of Rap1

To directly test whether CA leads to conversion of inactive GDP-bound Rap1 to the active GTP-bound state, a mechanism which has been reported to cause increased metastasis in cancer cells (Sit & Manser, 2011), an activated Rap1 pull-down assay was performed. Our findings showed that CA increased Rap1 activation in CA+ MCF10A (Fig. 2A).

Since Rap-1 also plays a key role in regulating cell-ECM contacts, (Sit & Manser, 2011) its mediation of CA-induced cellular effects was investigated using Rap1 pharmacological inhibitor (GGTI298). An adhesion assay using a type I collagen coated plate demonstrated a trend of increased cell-ECM attachment in +CA cells in comparison to -CA. Interestingly, blocking Rap1 activity for 3h using GGTI298 inhibitor significantly decreased this CA-induced effect (Fig. 2B). Similarly, the transwell *in vitro* assays demonstrated significantly greater invasion in +CA cells and that the inhibition of Rap1 significantly decreased both CA-induced cell invasion (Fig. 2C) and migration (Fig. 2D) in CA+ cells. These results highlight the possible involvement of a Rap1-mediated pathway in promoting CA-induced downstream tumorigenic events.

Study of epithelial barrier integrity using a modified long-term breast epithelial cell culture model

In cancer cells, cell adhesiveness is dysregulated, allowing cancer cells to ignore cellular norms, resulting in defective and altered histological structure promoting cancer invasion and metastasis (Hirohashi & Kanai, 2003).

No study has yet reported CA effects on epithelial barrier integrity and cell junction protein localisation expression, especially tight junctions (TJ) and desmosomes (DS). Therefore, we explored the role of CA in disruption of cell-cell adhesion and cell-ECM adhesion in promoting cancer spread. Since the untransformed breast epithelial cell line MCF10A has limitations in forming robust TJ under standard cell culture conditions due to low endogenous expression of polarity protein complex Crumbs3 (CRB3) (Fogg *et al*, 2005; Underwood *et al*, 2006) a modified long-term cell culture system was developed (Fig. 3A). MCF10A cells cultured for longer periods of time have the ability to form TJ under modified culture conditions, especially in the absence of the common MCF10A growth supplement cholera toxin (CT) (Marshall *et al*, 2009). Previous studies have reported that CA prevalence is usually higher in tumour cells in *in vivo* than *in vitro* conditions due to intratumoural hypoxia, and that cells with high CA levels *in vitro* are eliminated over time in a p53-dependent manner (Mittal *et al*, 2017). Hence, in the optimised 47-day MCF10A PLK4 WT cell culture, CA induction and persistence were ensured in long-term culture by pulsing the cells with +/-2 µg/ml DOX at the regular time intervals (Fig. 3A). % CA achieved was verified using γ-tubulin fluorescent labelling and CA effects on morphological barrier integrity and cell junction formation was extensively analysed using confocal and electron microscopy. In this multi-layered, apico-basally polarised cell culture system (Fig 3D), an average of 42% of cells at the apical region and 25% of cells in the middle layer harboured CA (Fig. 3B-C). The variation in % CA achieved in 2D vs long-term transwell culture is likely due to the multi-layer organisation of the MCF10A cells by day 47 (Fig 3D). Furthermore, the localization of β-catenin varied from highlighting well-ordered cortical rings in -CA cells to a disordered pattern of incomplete ring staining and focal condensations in +CA cells. Also of note, the sagittal TEM overview of 47-day multi-layered cell culture consistently revealed more intercellular space in -CA, while +CA apparently formed a compact cell organisation (more like a bilayer) with minimal intercellular space (Fig. 3D). Furthermore, confocal Z-stack projections of immunofluorescent staining of tight junction protein ZO-1 and adherens junction β-catenin showed localisation of both proteins at the apical side which was clearly disrupted in +CA conditions.

Centrosome Amplification alters epithelial cell-cell adhesion by disrupting junction barrier integrity and cell junction formation

We hypothesised that CA-induced migration and invasion of cells could be facilitated by a disruption of epithelial barrier integrity. Confocal microscopy analysis of a long-term MCF10A cell culture model further revealed that vehicle-treated MCF10A cells formed well-organised TJ on the apical side, as examined by immunofluorescent labelling TJ family proteins ZO-1, occludin and JAM-A and AJ protein β-catenin (Fig. 4A). CA effects on morphological epithelial barrier integrity was measured using two approaches: (i) measuring the average grey value intensity of each cell junction markers fluorescent intensity at the apical region for 10 fields of view. (ii) Binary quantification of cell junction disruption, where a well-formed continuous junction was scored as 1 and a disrupted or non-continuous cell junction was scored as zero and % disruption in the population was calculated. The +CA PLK4 cells showed a significant increase in grey value intensity value for each of β-catenin and JAM-

A and a decrease in each of ZO-1 and occludin signal intensity at the apical region (Fig. 4B). Furthermore, quantification of % cell junction protein disruption quantification using the same junctional markers revealed significant increase in overall epithelial cell junction disruption in +CA compared to -CA conditions (Fig. 4C). Correct localisation/orientation of cell junction proteins are required for maintaining epithelial cell polarity and maintaining epithelial barrier integrity. Our results from the long-term cell culture showed clear evidence of CA involvement in disrupting epithelial barrier integrity through mis or re-localisation of TJ proteins JAM-A, occludin and ZO-1 and adherens junction protein β-catenin in the apical lining cells of the cell layer.

We next investigated possible effects of CA on MCF10A cell junction formation at an ultra-structural level using transmission electron microscopy (Fig. 4D). We showed that the presence of CA in the population significantly reduced AJ formation at the cell-cell interface whilst also reducing tight junction and desmosome formation in CA+ cells. An interesting observation noted from the TEM images of cells cultured using the long-term model was that in both +/- CA conditions, the interior layers showed membrane protrusions and desmosomes were the major intercellular junction that connected the interior cells of the multi-layered epithelium. Subsequently, these findings were compared with CA negative control MCF10A 608 47-day cell culture, to ensure the results obtained were linked to CA induction and not due to off-target effects of PLK4 overexpression or DOX treatment (Fig. S3A&B). Doxycycline pulsing treatments in 47-day cultures of negative control MCF10A 608 cells did not cause dramatic cell junction disruption or protein mislocalisation, confirming that the results observed in +CA PLK4 cells were due to the presence of extra centrosomes.

A predominant cytoskeletal structural modification identified from TEM analysis was the long bundle of cytoskeletal microfilaments (intermediate filaments) noted in -CA conditions in close association with either intermediate cell junction (DS) compared to the severely truncated, wavey filaments observed in +CA cells (Fig. 5A). Additionally, it was also noted that +CA cells consistently displayed increased autophagosome or phagophore-like structures near deformed cell junctions (Fig. 5B&C). Intriguingly, this supports recent work by Denu et al, demonstrating that CA disrupts autophagy trafficking by modulating the microtubule network and increases the accumulation of autophagosomes in MCF10A cells (Denu *et al.*, 2020). CA effects on cytoskeletal structure and autophagy is based only on preliminary observations from images taken at 20,000X magnification and further detailed exploration of these CA-induced effects beyond the scope of the current manuscript is warranted.

Centrosome Amplification effects on epithelial cell-cell adhesion in MCF7 PLK4 model

Due to the limitations of MCF10A in readily forming cell junctions under standard cell culture conditions, the above results were further validated in the luminal A breast cancer cell line MCF7, the only known breast cancer cell line known to assemble tight junctions (albeit partial) under standard culture conditions (Zangari *et al*, 2014). Literature evidence has shown that TJ protein dysregulation in MCF7 cell lines promotes migratory/invasive

changes (McSherry *et al*, 2011). Like the MCF10A model used, the MCF7 PLK4 cell line is a genetically engineered variant which overexpresses wild-type PLK4 genes under the control of the tetracycline inducible system (Arnandis *et al.*, 2018). To test the CA effects in MCF7 cells, CA induction and cell junction quantification was performed as before but in a 10-day transwell cell culture (Fig. 6A) based on Sheller et al (Sheller *et al*, 2017).

Confocal microscopy analysis of MCF7 PLK4 on the apical side harbouring excess centrosomes did not show as significant a negative impact on cell junction protein localisation as in +CA MCF10A (Fig. 6B). Cell junction protein disruption % quantification using junctional markers ZO-1, JAM-A and occludin revealed a definite but non-significant disruption and mislocalisation of epithelial tight junction markers in the presence of CA (Fig. 6C). Diffusion of β-catenin away from the cortical membrane was also seen in + CA MCF7. In line with these findings, the TEM analysis on the same cells revealed that while CA had no effect on adherens or desmosome formation, there was a declining trend in TJ formation in +CA MCF7 cells. Thus, CA-induced alterations of cell junctions may be cell-type specific.

Centrosome amplification dysregulates major cell-cell junction and cell-ECM attachment regulating genes

To further explore CA effects on mechanisms of cell attachment, cell junction and cell adhesion total protein/gene expression was analysed by western blotting analysis and RT-PCR respectively. Considering the baseline low levels of TJ formation in MCF10A, these experiments were carried out in growth conditions lacking cholera toxin and CA effects on epithelial TJ protein expression were studied up to 4 days post-CA induction (Fig.7A). Our results show that induction of CA reduced total ZO-1 (5-fold) and total occludin protein (1.4-fold) from the TJ family (day-4) while CA induced a ~2-fold increase in AJ protein β-catenin post 48h (day-2). A 1.5-fold upregulation in the gap junction protein, connexin 43 was observed with CA induction. The desmosomal cadherin, desmoglein 1 displayed a 2-fold increase in total protein expression in response to CA whereas desmocollin was unaffected. Plakoglobin (also known as γ-catenin), an adaptor protein found in both desmosomes and adherens junctions was not affected by CA-induction. Therefore, induction of CA variably dysregulates the expression of cell junction molecules.

Having demonstrated CA-induced mislocalisation of TJ proteins at the apical region and altered epithelial barrier integrity using confocal microscopy, we hypothesised that CA disrupts cell junction protein subcellular localisation. Therefore, cell junction localisation in cytoskeletal (cyt), cytoplasmic (sol) and nuclear (nuc) fractions was further investigated ±CA. CA was associated with redistribution of occludin and β-catenin from the cytoskeletal to the nuclear fraction and with reduced recovery of JAM-A in cytoskeletal fraction (Fig. 7B). While ZO-1 localisation is seen to increase in the cytoskeletal fraction, the confocal and TEM analysis suggests that it is a punctate localisation which does not form a robust cell junction. Thus, altered cytoskeletal dynamics induced

by extra microtubule nucleation sites associated with the amplified centrosomes causes cell junction disruption at the protein expression, localisation and structural junction levels.

Cell-ECM attachment dysregulation also plays a critical role in cancer metastasis. qPCR profiler array data showed that of the 84 genes analysed, CA significantly dysregulated the expression of the cell-matrix adhesion molecule expression beta integrin 3 (ITGB3), its binding partner and ECM component fibronectin (FN1) and dysregulated the balance of ECM degrading enzymes Matrix metalloproteinases (MMP1, MMP13 and MMP16) and Tissue inhibitors of MMPs (TIMP1) which remodel the ECM during breast cancer cell invasion. This shows that CA acts as a potential early trigger of this established cell invasion pathway.

DISCUSSION

CA is a known hallmark of cancer detected in a range of human solid and haematological malignancies, particularly associated with increased tumour aggressiveness, poor survival and metastatic cancer subtypes (Chan, 2011; Denu *et al*, 2016). The current study adds to mounting evidence that CA plays a causal role in the pathogenesis of cancer (reviewed in (Rhys & Godinho, 2017)). Here we show that CA initiates the early genesis of invasive change by promoting cell migration and invasiveness *in vitro*, independent of the mechanism of induction (PLK4 overexpression or CDK1 inhibition). This work quantifies the dissemination of tumour cells out of the epithelial layer via a combination of cell autonomous and non-cell-autonomous effects of CA shown in previous studies (Arnandis *et al.*, 2018; Godinho *et al.*, 2014). *In vivo* validation was done in the Chick embryo xenograft model, an emerging alternative *in vivo* model system which is gaining broad acceptance due to its rapidity, simplicity and fewer ethical issues (discussed in (Harper *et al*, 2021)). Using this system, we show the earliest observable effects of triggering CA *in vivo* on a control breast epithelial background, with evidence of cell invasion of MCF10A into the chicken mesodermis, hyperplasia of the chorionic epithelium at the interface with the Matrigel-cell graft, heterophil infiltrates (the avian heterologues of neutrophils) and dilated lymphatics in the presence of the CA-harbouring MCF10A xenografts. Furthermore, secondary tumour-associated characteristics of hemorrhaging, central necrosis and calcification were observed at the graft-host interface only in CA+ samples. Therefore, induction of CA on a control background triggers extensive tumour-like characteristics within days, confirming its contribution to tumour initiation in light of longer term tumourigenesis in mouse models (Coelho *et al.*, 2015; Levine *et al.*, 2017; Sercin *et al.*, 2016).

Signalling pathways involving small GTPases, Rho and Ras, frequently shown to be dysregulated in tumours, have previously been proposed to mediate CA-induced cellular effects. The Rho subfamily consisting of Rho A, Rac1, Cdc42 is well known for regulating cytoskeleton and actin dynamics, and Rac1 has been associated with lamellipodia formation during cell migration (Sit & Manser, 2011). Increased microtubule nucleation by supernumerary centrosomes upon CA induction leads to increased Rac1 activity which promotes actin polymerisation disrupting cell adhesion and promoting cell invasion (Godinho *et al.*, 2014). In addition, small

GTPase Ras-associated protein Rap1 is highly expressed in cancer cells, stimulating integrin mediated cell-ECM attachment, matrix metalloproteinase expression involved in ECM remodelling and cytoskeletal modulation, paving way for cancer cell invasion and migration (Zhang *et al*, 2017). Rap 1 acts as a tumour promoter mediating metastasis in a range of cancer contexts including breast, prostate, ovarian, oesophageal and pancreatic cancers (reviewed in (Looi *et al*, 2020)). We found that induction of CA increases the levels of active GTP-bound Rap1 and that pharmacological inhibition of Rap1 significantly decreases CA-dependent cell-ECM attachment, migration and invasion *in vitro*. Rap-1 inhibition in the chicken xenograft blocked CA+ MCF10A invasion, hyperplasia of chorionic epithelium and dilation of lymphatics and blood vessels, displaying a phenotype resembling the -CA MCF10A xenograft. Therefore, in addition to Rac1, Rap1 GTPase plays a key role in the signalling pathways mediating CA induction of an invasive phenotype in control breast epithelial cells.

Our work shows that CA in an untransformed epithelial background is sufficient to trigger migration and invasion *in vitro* and *in vivo*, in conjunction with elevated cell-ECM attachment. Previous work has shown that tumourigenesis is associated with dramatic alterations in integrin expression profiles with these adhesion molecules facilitating cell movement by forming focal adhesions between cancer cells and the ECM (reviewed in (Hamidi & Ivaska, 2018). In breast cancer, integrin β3 overexpression (bound to subunit αv to form αvβ3 integrin) is associated with high metastatic potential, especially in promoting bone metastasis (Carter *et al*, 2015; Havaki *et al*, 2007; Kovacheva *et al*, 2021). Integrin β3 overexpression in breast epithelia paves the way for invading cells by inducing secretion of matrix metalloproteases MMP1 and 2 with resultant matrix degradation. Our data show CA-induced upregulation of gene expression of ITGB3 alongside that of its ECM binding partner fibronectin, and dysregulation of the balance of ECM degrading enzymes matrix metalloproteinases (MMP1, MMP13 and MMP16) and Tissue inhibitors of MMPs (TIMP1). Our hypothesis that these effects contribute to the observed effects of CA on cell invasion *in vivo* and *in vitro* are supported by clinical studies reporting high fibronectin expression in metastatic breast cancer in association with high MMP expression levels (Das *et al*, 2008; Fernandez-Garcia *et al*, 2014). Furthermore, fibronectin binding to integrin β1 heterodimeric receptors stimulates production of MMP-1 inducing an MMP-1-dependent invasive phenotype in breast cancer cells (Jia *et al*, 2004).

The formation of apico-basal polarised epithelia is closely coupled to cell-cell adhesion events at the apical junctional complex (AJC) consisting of tight junctions (TJ or zonula occludens) and sub-adjacent adherens junctions (AJ or zonula adherens)(Wang & Margolis, 2007). TJs perform both gate and fence functions, the former acting as a semi-permeable adhesive barrier regulating traffic through the paracellular space and the latter physically segregating lipids between apical and basolateral membrane compartments. AJs contribute to cell-cell adhesion via an adhesive belt lying basally to TJs. The cytoplasmic domains of the proteins that comprise AJC junctions are tethered to the cytoskeleton via various adaptor proteins integrating signals to regulate cell polarity and movement. Using our newly established MCF10A long-term cell culture model system, we observed

disruption and mislocalisation of both TJ and AJ components in the presence of CA, with an accompanying decrease in the numbers of AJCs formed between cells. Observed subcellular mislocalisation of JAM-A, occludin and β-catenin away from the cytoskeleton as well as overloading of ZO-1 protein at the cytoskeleton in CA+ cell populations, is a likely underlying cause of disrupted of cell-cell adhesion at cell junctions. The hypothesis is that excessive centrosome numbers impact on the cytoskeleton protein dynamics via elevated microtubule nucleation followed by actin polymerisation (Godinho *et al.*, 2014). Intriguingly, microtubule polymerisation inhibitors (MTIs) can re-establish functional AJCs in cell-cell adhesion-defective carcinoma cells via mechanosensitive recruitment of junction molecules (Ito *et al*, 2017). In this case, GTPase RhoA was found to be upregulated by MTIs, restoring AJCs by causing actomyosin contraction at the apical cortex and tension-dependent junction reassembly. The possibility that the opposite effect may be happening in our CA+ cells with elevated Rap1-GTP regulating RhoA activity remains to be explored.

The treatment of transformed cancer cell lines with PLK4 inhibitor Centrinone B to decrease inherent CA and reverse CA-induced phenotypes has previously been demonstrated (Denu *et al.*, 2020; Denu *et al.*, 2018; Wong *et al.*, 2015). In the current study, differential effects Centrinone on invasive capabilities of the cells correlated with endogenous CA levels, where the confirmed contribution of CA to migration and invasion of triple negative MDA-MB-231 breast epithelial cells (high CA) was not recapitulated in MDA-MB-468 (low CA). This indicates that across cancer cell subtypes, there are varying contributions from CA and other cellular mechanisms driving invasive capacity.

In conclusion, we found that CA induces tumorigenic changes in breast epithelial contexts *in vitro* and *in vivo,* promoting the transition to an invasive phenotype via disruption of cell-cell contacts and release of stromal proteases to facilitate destruction of the basement membrane and increased motility of invasive cells through the ECM. The in vivo finding that CA is sufficient to confer such advanced tumourigenic changes within days, identifies CA as an early driver alteration in cancer and a central targetable mechanism.

ACKNOWLEDGMENTS
The authors would like to acknowledge the Hardiman scholarship, NUI Galway, CMNHS Millennium fund and School of Medicine, NUI Galway for financial support. SHV was supported by Science Foundation Ireland grant 13/IA/1994 (to AMH).
Imaging in this project was carried out in the Centre for Microscopy & Imaging at the National University of Ireland, Galway (www.imaging.nuigalway.ie), a facility that is funded by NUIG and the Irish Government's Programme for Research in Third Level Institutions, Cycles 4 and 5, National Development Plan 2007-2013.

DECLARATION OF INTERESTS
The authors report no conflicts of interest.

MATERIALS AND METHODS

Cell culture and drug treatment

Wild type MCF10A and doxycycline-inducible PLK4 cell lines (MCF10A PLK4, MCF10A 608 (Godinho *et al.*, 2014)) were used to model CA in an untransformed breast cell context following 48h doxycycline at 2 mg/mL. MCF10A were cultured in Dulbecco's Modified Eagles' Medium/F-12 media supplemented with 5% Horse serum (Sigma 14M175/ H1270), 0.5µg/ml Hydrocortisone (Sigma H0888), 100ng/ml Cholera Toxin (Sigma C8052), 20ng/ml human Epidermal Growth Factor (hEGF) (Sigma E9644), 10µg/ml Insulin (Sigma I9278) 1% Penicillin/Streptomycin (Sigma P4333). The breast cancer cell lines MDA MB 231, MDA MB 468 and MCF7 cells were cultured in RPMI-1640 media (Sigma R8758) supplemented with 10% Fetal Bovine Serum (Sigma F7524) and 1% Penicillin/Streptomycin (Sigma P4333). All cell lines were maintained at 37 °C and 5% CO2. For CA induction, cells were treated for 48h with 2µg/ml Doxycycline hyclate (Sigma D9891) or 10µM CDK1 inhibitor RO3306. 150nM Centrinone B treatment for 16 h was used to inhibit CA. Vehicle controls were dH_2O for Dox treatments or DMSO for RO3306 and Centrinone B. Rap1 inhibition was achieved by pre-treating cells for 3 h with 10 µM GGTI298 (Biotechne Tocris 2430) and DMSO used as vehicle control.

Immunofluorescence staining and CA quantification

For CA quantification, the cells were cultured on Poly-D-Lysine (Sigma P7280) coated sterile coverslips. 48h after CA induction the coverslips were fixed in 2 ml chilled Methanol/EGTA (5mM) (Sigma E4378) at -20°C. The cells were incubated with the primary antibody of centrosome (γ-tubulin Sigma T3559) and cytoskeletal (α-tubulin Sigma B512) markers and stained with secondary antibodies (AlexaFlour® 594 Invitrogen A-11005, AlexaFlour® 488 anti-rabbit Invitrogen A-11008). Coverslips were mounted using Vectashield + DAPI (Vector Laboratories H-1200) and sealed with nail varnish and stored at 4ºC. Centrosomes were quantified by eye in >200 cells per slide and centrosome complement categorised as normal for 1-2 centrosomes/cell or numerically amplified if ≥3.

Cell invasion and migration assays

Transwell inserts with 8-µm pore membranes (Corning 353097) were used to assess CA effect on cellular invasion and migratory capacity. MCF10A were serum-deprived (1% horse serum and no hEGF) overnight (16h) and CA induced for 48h with 2 µg/ml DOX. Cells were seeded on transwell filters - uncoated to quantify cell migration or coated with matrigel (Corning™ 356231) for invasion. For 0 gradient controls, serum-deprived media (1% horse serum and no hEGF) was added to the upper and lower chambers. To create a chemoattractant gradient, complete media containing 6 % horse serum and 20 ng/ml hEGF was added to the lower chamber. Cells were incubated for 12 h and 24h for migration and invasion respectively. Cells located on the underside of the filter were stained with the crystal violet solution (Sigma HT901-8FOZ). Brightfield images from five different fields of view per insert were taken under 20X magnification. The number of migrated and invaded cells were quantified manually using ImageJ software wand tool (Schneider *et al*, 2012).

Chicken Embryo Xenograft Model

Fertilised chicken eggs (Breed: Ross 308, 3 eggs per treatment) were incubated at 37°C and 65% humidity. On embryonic development (ED) day 3, a window was created (sterile forceps and scissor used) on the eggshell under a heat lamp and approximately 2.5ml egg albumin was aspirated out. The eggs were re-sealed with transparent adhesive film (Opsite Flexifix™, Smith-Nephew). On ED day 8, a sterile silica ring was placed onto the chicken membrane and $2x10^6$ cells in 100µl of 1X PBS:Matrigel (Corning: 354248; 50:50 ratio) implanted. On ED 13,

the embryos were sacrificed, and the cell-matrigel graft with attached chorioallantoic membrane (CAM) harvested. The excised tissue images were observed using a stereo microscope (Leica S6E), gross images captured and the tissue transferred to the Thermo Scientific™ Excelsior Tissue Processor unit for standard overnight (14 h) fixation and paraffin-embedding. 5µm tissue sections were prepared using a Microtome (Microm HM325, Thermo Scientific), mounted and stained with haematoxylin and eosin stain (H&E) and visualised by brightfield microscopy at 40x on the Olympus VS120 Virtual Slide Scanner Microscope.

Immunohistostaining of xenograft tissue sections

The Cytokeratin 8 monoclonal antibody, (Cytokeratin CAM 5.2 BDBiosciences-345779) was used to label MCF10A cell invasion into the CAM. After deparaffinising and blocking, the slides were incubated with anti-Cyt5 antibody, HRP-conjugated secondary followed by 3,3'-Diaminobenzidine (DAB) staining using the ImmPRESS™ Excel Amplified HRP peroxidase Polymer Staining Kit (Vector Laboratories MP-7602-15) manufacturer protocol. Cytokeratin CAM 5.2 does not require an antigen retrieval step. All images were captured with brightfield microscopy at 40x on the Olympus VS120 Virtual Slide Scanner Microscope.

Long term cell culture on transwell semi-permeable membrane inserts

Long-term cell culture was established based on (Marshall *et al.*, 2009) to investigate CA effects on apical junctional complex formation. MCF10A PLK4/608 cells cultured in complete DMEM/F12 medium in the absence of cholera toxin (CT) were seeded onto the transwell inserts ($1.2x10^5$ cells, growth area $1.1cm^2$ and pore size of 0.4 µm). The cells were maintained for up to 47 days by replacing media in both chambers every 48h. For IF staining, transwell inserts were sliced in quarters with a sharp scalpel blade, mounted and fixed with 3.7% paraformaldehyde and permeabilised with 0.5% Triton X. IF was performed with cell junction primary antibodies JAM-A (sc-53623), β-Catenin (sc-7963), Occludin (Invitrogen 71-1500), ZO-1 (Invitrogen 61-7300) and secondary antibodies (AlexaFlour® 594 Invitrogen A-11005, AlexaFlour® 488 anti-rabbit Invitrogen A-11008). Filters and coverslips were mounted with Vectashield + DAPI and images captured with a Andor spinning disk confocal microscopy under 60X magnification. The cell junction integrity on the apical side was quantified using binary scoring method, 1 = intact cell junction and 0 = disrupted cell junction. Cell junction localisation was quantified using the value intensity (grey scale of each channel) of cell junctions marked by β-Catenin, ZO-1, JAM-A and Occludin, using ImageJ software.

Transmission electron microscopy (TEM)

The long-term MCF10A PLK4WT/608 filter inserts were washed in 1X PBS and fixed in primary fixative solution containing 2% glutaraldehyde (Sigma G5882), 2% paraformaldehyde (Fisher Scientific 10131580) in 0.1M sodium cacodylate pH 7.2(Sigma C0250). Following washes with 0.2M sodium cacodylate buffer, filters were incubated in secondary fixative 1% osmium tetroxide in 0.1M sodium cacodylate buffer (pH 7.2)). Filters were dehydrated through a graded series of ethanols and infiltrated with resin: acetone mixtures overnight (50:50 mixture, 75:25 mixture and 100% resin). Filters were finally polymerised in 100% resin and ultra-thin (70-90nm) sections were cut in a sagittal plane using a diamond knife and mounted onto 3mm copper grids. The grids were counterstained with UA Zero non-radioactive EM Stain (Agar Scientific AGR1000) and visualised on a Hitachi 7500 TEM microscope. For cell junction quantification, the images were taken under 20,000X magnification. The cell junctions were counted from minimum 15 images per TEM grid and a score of 1 and 0.5 was assigned to normal and deformed cell junctions respectively.

Subcellular fractionation analysis and Western blotting

A cytoskeletal protein extraction was performed as described in (Choi *et al*, 2014). Briefly, cells were lysed in buffer containing 50mM PIPES, 50 mM NaCl, 5% Glycerol, 0.1% NP-40, 0.1% Triton X-100 and 0.1% Tween 20 with a protease inhibitor cocktail. The lysis buffer (cytoplasmic fraction) was retained, and the cells were rinsed with 5 ml of 50mM Tris-HCl (pH 7.4) and nuclease buffer containing 10 U/mL Benzonase® Nuclease (Sigma E1014), 10 mM MgCl2 and 2 mM CaCl2 in 50 mM Tris-HCl buffer, pH 7.5. The nuclease buffer was retained (nuclear fraction), and cytoskeletal proteins collected by solubilising in 0.5 ml of 1% SDS.
The protein concentration was determined by Pierce™ Bicinchoninic acid (BCA) Protein Assay. Western blot assay was carried out following standard protocols, 30 µg and 60 µg protein were used for semi-dry and wet transfer respectively. Antibodies used were JAM-A sc-53623 (1:500), β-Catenin sc-7963 (1:1000), Occludin Invitrogen 71-1500 (1:1000), ZO-1 Invitrogen 61-7300 (1:1000), Plakoglobin BD 61025 (1:1000), Desmoglein-1 BD 610273 (1:500), Desmocollin 2/3 Zymed 32-6200 (1:500), Connexin 43 Proteintech 15386-1-AP (1:500), anti-Actin Sigma-Aldrich A2066 (1:5000), anti-GAPDH Sigma-Aldrich G9545 (1:5000), HRP-conjugated anti-mouse and rabbit - Jackson Laboratories (1:5000).

Rap-1 Activation Pull-down Assay

Cells were trypsinised at 80% confluency and $2x10^6$ MCF10A cells were seeded to the $175cm^2$ flasks. Post-16h of cell seeding, CA was induced with 2µg/ml Dox for 48 hours. The assay was performed using the Rap1 Activation Assay Kit (17-321 Sigma-Aldrich) according to the manufacturer's instructions.

RNA preparation and real-time quantitative PCR (qPCR)

The Qiagen RT2 Profiler PCR Array for 84 Cell Adhesion and Extracellular Matrix molecules (Catalogue no. - PAHS-013Z) was used and the PCR component mix for 96 well plate prepared according to manufacturer's instructions. The experiment was performed as per the Profiler array format C protocol on a StepOnePlus™ Real-Time PCR System (Applied Biosystems). Data analysis was carried out using the Qiagen GeneGlobe RT-qPCR Data Analysis web tool.

Cell adhesion assay

The assay was performed as previously described (Chen, 2012). CA was induced in MCF10A PLK4 by adding 2µg/ml DOX. After 48 h of CA induction and overnight serum starvation, cells were added to type I collagen (Corning™ 354231) (positive control) or 1% BSA (negative control) coated 96 well plates and incubated for 20 min. After a series of washing steps, the cells bound to the substrate were analysed and quantified by crystal violet staining.

Statistical analyses

All statistical comparisons were performed with GraphPad® Prism 9 (www.graphpad.com). Depending on the number of factors, multiple-group comparisons were made using either a single or two-way analysis of variance (ANOVA) followed by the Bonferroni test to confirm statistical differences between groups. Paired sample analysis was performed using a two-sided unpaired or paired Student's t-test. Statistical significance (p-value) was assigned for values <0.05.

REFERENCES

Adams SD, Csere J, D'Angelo G, Carter EP, Romao M, Arnandis T, Dodel M, Kocher HM, Grose R, Raposo G *et al* (2021) Centrosome amplification mediates small extracellular vesicle secretion via lysosome disruption. *Curr Biol* 31: 1403-1416 e1407

Arnandis T, Monteiro P, Adams SD, Bridgeman VL, Rajeeve V, Gadaleta E, Marzec J, Chelala C, Malanchi I, Cutillas PR *et al* (2018) Oxidative Stress in Cells with Extra Centrosomes Drives Non-Cell-Autonomous Invasion. *Dev Cell* 47: 409-424 e409

Bettencourt-Dias M (2013) Q&A: Who needs a centrosome? *BMC Biol* 11: 28

Bettencourt-Dias M, Rodrigues-Martins A, Carpenter L, Riparbelli M, Lehmann L, Gatt MK, Carmo N, Balloux F, Callaini G, Glover DM (2005) SAK/PLK4 is required for centriole duplication and flagella development. *Curr Biol* 15: 2199-2207

Bornens M (2012) The centrosome in cells and organisms. *Science* 335: 422-426

Bourke E, Brown JA, Takeda S, Hochegger H, Morrison CG (2010) DNA damage induces Chk1-dependent threonine-160 phosphorylation and activation of Cdk2. *Oncogene* 29: 616-624

Bourke E, Dodson H, Merdes A, Cuffe L, Zachos G, Walker M, Gillespie D, Morrison CG (2007) DNA damage induces Chk1-dependent centrosome amplification. *EMBO Rep* 8: 603-609

Buglak DB, Kushner EJ, Marvin AP, Davis KL, Bautch VL (2020) Excess centrosomes disrupt vascular lumenization and endothelial cell adherens junctions. *Angiogenesis* 23: 567-575

Carter RZ, Micocci KC, Natoli A, Redvers RP, Paquet-Fifield S, Martin AC, Denoyer D, Ling X, Kim SH, Tomasin R *et al* (2015) Tumour but not stromal expression of beta3 integrin is essential, and is required early, for spontaneous dissemination of bone-metastatic breast cancer. *J Pathol* 235: 760-772

Chan JY (2011) A clinical overview of centrosome amplification in human cancers. *Int J Biol Sci* 7: 1122-1144

Chen Y (2012) Cell Adhesion Assay. *Bio-Protocol* 2

Choi S, Kelber J, Jiang X, Strnadel J, Fujimura K, Pasillas M, Coppinger J, Klemke R (2014) Procedures for the biochemical enrichment and proteomic analysis of the cytoskeletome. *Anal Biochem* 446: 102-107

Coelho PA, Bury L, Shahbazi MN, Liakath-Ali K, Tate PH, Wormald S, Hindley CJ, Huch M, Archer J, Skarnes WC *et al* (2015) Over-expression of Plk4 induces centrosome amplification, loss of primary cilia and associated tissue hyperplasia in the mouse. *Open Biol* 5: 150209

Cosenza MR, Kramer A (2016) Centrosome amplification, chromosomal instability and cancer: mechanistic, clinical and therapeutic issues. *Chromosome Res* 24: 105-126

Das S, Banerji A, Frei E, Chatterjee A (2008) Rapid expression and activation of MMP-2 and MMP-9 upon exposure of human breast cancer cells (MCF-7) to fibronectin in serum free medium. *Life Sci* 82: 467-476

Denu RA, Kaur G, Sass MM, Lakkaraju A, Burkard ME (2020) Centrosome Amplification in Cancer Disrupts Autophagy and Sensitizes to Autophagy Inhibition. *Mol Cancer Res* 18: 33-45

Denu RA, Shabbir M, Nihal M, Singh CK, Longley BJ, Burkard ME, Ahmad N (2018) Centriole Overduplication is the Predominant Mechanism Leading to Centrosome Amplification in Melanoma. *Mol Cancer Res* 16: 517-527

Denu RA, Zasadil LM, Kanugh C, Laffin J, Weaver BA, Burkard ME (2016) Centrosome amplification induces high grade features and is prognostic of worse outcomes in breast cancer. *BMC Cancer* 16: 47

Dodson H, Bourke E, Jeffers LJ, Vagnarelli P, Sonoda E, Takeda S, Earnshaw WC, Merdes A, Morrison C (2004) Centrosome amplification induced by DNA damage occurs during a prolonged G2 phase and involves ATM. *EMBO J* 23: 3864-3873

Farina F, Gaillard J, Guerin C, Coute Y, Sillibourne J, Blanchoin L, Thery M (2016) The centrosome is an actin-organizing centre. *Nat Cell Biol* 18: 65-75

Fernandez-Garcia B, Eiro N, Marin L, Gonzalez-Reyes S, Gonzalez LO, Lamelas ML, Vizoso FJ (2014) Expression and prognostic significance of fibronectin and matrix metalloproteases in breast cancer metastasis. *Histopathology* 64: 512-522

Fogg VC, Liu CJ, Margolis B (2005) Multiple regions of Crumbs3 are required for tight junction formation in MCF10A cells. *J Cell Sci* 118: 2859-2869

Fujiwara T, Bandi M, Nitta M, Ivanova EV, Bronson RT, Pellman D (2005) Cytokinesis failure generating tetraploids promotes tumorigenesis in p53-null cells. *Nature* 437: 1043-1047

Ganem NJ, Godinho SA, Pellman D (2009) A mechanism linking extra centrosomes to chromosomal instability. *Nature* 460: 278-282

Ganier O, Schnerch D, Nigg EA (2018) Structural centrosome aberrations sensitize polarized epithelia to basal cell extrusion. *Open Biol* 8
Garcia MA, Nelson WJ, Chavez N (2018) Cell-Cell Junctions Organize Structural and Signaling Networks. *Cold Spring Harb Perspect Biol* 10
Godinho SA, Picone R, Burute M, Dagher R, Su Y, Leung CT, Polyak K, Brugge JS, Thery M, Pellman D (2014) Oncogene-like induction of cellular invasion from centrosome amplification. *Nature* 510: 167-171
Habedanck R, Stierhof YD, Wilkinson CJ, Nigg EA (2005) The Polo kinase Plk4 functions in centriole duplication. *Nat Cell Biol* 7: 1140-1146
Hamidi H, Ivaska J (2018) Every step of the way: integrins in cancer progression and metastasis. *Nat Rev Cancer* 18: 533-548
Harper K, Yatsyna A, Charbonneau M, Brochu-Gaudreau K, Perreault A, Jeldres C, McDonald PP, Dubois CM (2021) The Chicken Chorioallantoic Membrane Tumor Assay as a Relevant In Vivo Model to Study the Impact of Hypoxia on Tumor Progression and Metastasis. *Cancers (Basel)* 13
Havaki S, Kouloukoussa M, Amawi K, Drosos Y, Arvanitis LD, Goutas N, Vlachodimitropoulos D, Vassilaros SD, Katsantoni EZ, Voloudakis-Baltatzis I *et al* (2007) Altered expression pattern of integrin alphavbeta3 correlates with actin cytoskeleton in primary cultures of human breast cancer. *Cancer Cell Int* 7: 16
Hirohashi S, Kanai Y (2003) Cell adhesion system and human cancer morphogenesis. *Cancer Sci* 94: 575-581
Ito S, Okuda S, Abe M, Fujimoto M, Onuki T, Nishimura T, Takeichi M (2017) Induced cortical tension restores functional junctions in adhesion-defective carcinoma cells. *Nat Commun* 8: 1834
Jia Y, Zeng ZZ, Markwart SM, Rockwood KF, Ignatoski KM, Ethier SP, Livant DL (2004) Integrin fibronectin receptors in matrix metalloproteinase-1-dependent invasion by breast cancer and mammary epithelial cells. *Cancer Res* 64: 8674-8681
Kessenbrock K, Plaks V, Werb Z (2010) Matrix metalloproteinases: regulators of the tumor microenvironment. *Cell* 141: 52-67
Kovacheva M, Zepp M, Berger S, Berger MR (2021) Conditional knockdown of integrin beta-3 reveals its involvement in osteolytic and soft tissue lesions of breast cancer skeletal metastasis. *J Cancer Res Clin Oncol* 147: 361-371
Levine MS, Bakker B, Boeckx B, Moyett J, Lu J, Vitre B, Spierings DC, Lansdorp PM, Cleveland DW, Lambrechts D *et al* (2017) Centrosome Amplification Is Sufficient to Promote Spontaneous Tumorigenesis in Mammals. *Dev Cell* 40: 313-322 e315
Looi CK, Hii LW, Ngai SC, Leong CO, Mai CW (2020) The Role of Ras-Associated Protein 1 (Rap1) in Cancer: Bad Actor or Good Player? *Biomedicines* 8
Lopes CAM, Mesquita M, Cunha AI, Cardoso J, Carapeta S, Laranjeira C, Pinto AE, Pereira-Leal JB, Dias-Pereira A, Bettencourt-Dias M *et al* (2018) Centrosome amplification arises before neoplasia and increases upon p53 loss in tumorigenesis. *J Cell Biol* 217: 2353-2363
Marshall AM, Pai VP, Sartor MA, Horseman ND (2009) In vitro multipotent differentiation and barrier function of a human mammary epithelium. *Cell Tissue Res* 335: 383-395
Marteil G, Guerrero A, Vieira AF, de Almeida BP, Machado P, Mendonca S, Mesquita M, Villarreal B, Fonseca I, Francia ME *et al* (2018) Over-elongation of centrioles in cancer promotes centriole amplification and chromosome missegregation. *Nat Commun* 9: 1258
McSherry EA, Brennan K, Hudson L, Hill AD, Hopkins AM (2011) Breast cancer cell migration is regulated through junctional adhesion molecule-A-mediated activation of Rap1 GTPase. *Breast Cancer Res* 13: R31
Mittal K, Choi DH, Ogden A, Donthamsetty S, Melton BD, Gupta MV, Pannu V, Cantuaria G, Varambally S, Reid MD *et al* (2017) Amplified centrosomes and mitotic index display poor concordance between patient tumors and cultured cancer cells. *Sci Rep* 7: 43984
Pihan GA, Wallace J, Zhou Y, Doxsey SJ (2003) Centrosome abnormalities and chromosome instability occur together in pre-invasive carcinomas. *Cancer Res* 63: 1398-1404
Rhys AD, Godinho SA (2017) Dividing with Extra Centrosomes: A Double Edged Sword for Cancer Cells. *Adv Exp Med Biol* 1002: 47-67
Sahai E, Olson MF, Marshall CJ (2001) Cross-talk between Ras and Rho signalling pathways in transformation favours proliferation and increased motility. *EMBO J* 20: 755-766
Schneider CA, Rasband WS, Eliceiri KW (2012) NIH Image to ImageJ: 25 years of image analysis. *Nat Methods* 9: 671-675

Segat D, Cassaro M, Dazzo E, Cavallini L, Romualdi C, Salvador R, Vitale MP, Vitiello L, Fassan M, Rugge M *et al* (2010) Pericentriolar material analyses in normal esophageal mucosa, Barrett's metaplasia and adenocarcinoma. *Histol Histopathol* 25: 551-560
Sercin O, Larsimont JC, Karambelas AE, Marthiens V, Moers V, Boeckx B, Le Mercier M, Lambrechts D, Basto R, Blanpain C (2016) Transient PLK4 overexpression accelerates tumorigenesis in p53-deficient epidermis. *Nat Cell Biol* 18: 100-110
Sheller RA, Cuevas ME, Todd MC (2017) Comparison of transepithelial resistance measurement techniques: Chopsticks vs. Endohm. *Biol Proced Online* 19: 4
Sit ST, Manser E (2011) Rho GTPases and their role in organizing the actin cytoskeleton. *J Cell Sci* 124: 679-683
Steere N, Wagner M, Beishir S, Smith E, Breslin L, Morrison CG, Hochegger H, Kuriyama R (2011) Centrosome amplification in CHO and DT40 cells by inactivation of cyclin-dependent kinases. *Cytoskeleton (Hoboken)* 68: 446-458
Underwood JM, Imbalzano KM, Weaver VM, Fischer AH, Imbalzano AN, Nickerson JA (2006) The ultrastructure of MCF-10A acini. *J Cell Physiol* 208: 141-148
Vasileva E, Citi S (2018) The role of microtubules in the regulation of epithelial junctions. *Tissue Barriers* 6: 1539596
Wang Q, Margolis B (2007) Apical junctional complexes and cell polarity. *Kidney Int* 72: 1448-1458
Wong YL, Anzola JV, Davis RL, Yoon M, Motamedi A, Kroll A, Seo CP, Hsia JE, Kim SK, Mitchell JW *et al* (2015) Cell biology. Reversible centriole depletion with an inhibitor of Polo-like kinase 4. *Science* 348: 1155-1160
Zangari J, Partisani M, Bertucci F, Milanini J, Bidaut G, Berruyer-Pouyet C, Finetti P, Long E, Brau F, Cabaud O *et al* (2014) EFA6B antagonizes breast cancer. *Cancer Res* 74: 5493-5506
Zhang YL, Wang RC, Cheng K, Ring BZ, Su L (2017) Roles of Rap1 signaling in tumor cell migration and invasion. *Cancer Biol Med* 14: 90-99

FIGURE LEGENDS

Figure 1: CA increases *in vitro* and *in vivo* migration and invasion of MCF10A PLK4 WT cells and blocking CA decreased metastatic characteristics in TNBC cell line MDA-MB-231. (A) Fluorescence microscopy quantification of CA induction - normal centrosome number (≤2 per cell) and amplified centrosomes or CA (≥2 per cell). CA was induced with 2µg +/- DOX treatment for the indicated time course and cells fixed with Methanol/5mM EGTA solution and stained for microtubules (α-tubulin, red), centrosomes (γ-Tubulin, green) and counterstained with DAPI (DNA, blue). Scale bar = 10 µm. Images are representative of n=3 independent experiments. (B) Bar graph shows % of cells exhibiting CA at each time point post DOX treatment, 48h was chosen as the optimal time point with CA of 80%. Error bars represent mean ± sem from 3 independent experiments; 200 cells counted per time point. (C) Transwell invasion assay and (D) migration assays results show that CA induction significantly increased cellular invasion and migration in MCF10A PLK4 cells compared to controls -CA PLK4 and + DOX PLK4 608. The bar graph represents mean number of cells invaded and migrated. Error bars represent mean ± sem from four independent experiments. One-way ANOVA and Bonferroni's multiple comparison test was used to determine significance, *P ≤ 0.05, ** P ≤ 0.01. (E) Representative images of chicken xenograft assay with cell-matrigel graft. Images show Haemotoxylin & Eosin (H&E upper panels) with Matrigel staining pink and immunohistochemical staining for Cytokeratin 5 (Cy5: lower panels) on formalin-fixed paraffin-embedded tissue sections ±CA MCF10A PLK4 cells/matrigel grafts. The + CA graft shows moderate to strong chicken-graft focal reaction (red arrows) and epithelial cell nests in chicken mesodermal layer (black arrows); only a mild to moderate focal reaction was noted in - CA grafts. The corresponding IHC showed epithelial cell nests were positive for Cy5 (dotted circles). Scale bar = 500µm. (F) Transwell invasion and (G) migration assay to assess the contribution of CA to the invasive phenotype of TNBC cell line MDA MB 23. Blocking CA with 150nM Centrinone B for 16 hours significantly decreased cellular invasion and migration. Migrated or invaded cells were quantified with DAPI staining and the cells counted from five different fields at 20X magnification. Error bars represent ± SEM values from two independent biological repeats, Student T-test was used to determine the statistical significance *P ≤ 0.05, *** P < 0.001.

Figure 2: CA increases Rap1 activity and Rap-1 activation mediates CA+ MCF10A invasion, migration and cell-ECM attachment. (A) Western blot of Rap1 pull-down assay shows CA increased GTP-bound Rap-1 in + CA compared to - CA. The image shown is representative of n=2 independent repeats. (B) CA increases MCF10A cell-ECM contact in a Rap1-dependent manner. MCF10A PLK4 cells were harvested after 48h treatment with +/- 2 µg/ml DOX and 3h treatment with +/- 10µM GGTI 298, and cell adhesion assays performed. Post 4h incubation, cells bound to the collagen matrix were stained with crystal violet. Cells from five 20X fields per well were counted and the bar graph represents mean ± SEM from four independent experiments. Two-way ANOVA was used to determine statistical significance, **P ≤ 0.01. Rap1 inhibition significantly decreased CA-induced cellular invasion (C) and migration (D). The bar graphs represent mean number of cells invaded and migrated, quantified by DAPI staining in five random 20X fields per insert. Error bars represent mean ± SEM

from four independent experiments and two-way ANOVA and Bonferroni's multiple comparison test was used to determine the significance, * $P \leq 0.05$, **$P \leq 0.01$. (E) Representative H&E images of chicken xenograft assay with cell-matrigel graft. MCF10A PLK4 cells were xenografted after 48h treatment with +/- 2 µg/ml DOX and 3h treatment with +/- 10µM GGTI 298. Rap-1 inhibition decreased the +CA bidirectional chicken-graft reaction. Scale bar = 500µm.

Figure 3: Advanced microscopy analysis of 47-day long term MCF10A PLK4 WT cell culture (A) Experimental layout of long-term transwell membrane cell culture system. (B) Representative immunofluorescent images of MCF10A PLK4WT cells cultured for 47 days. CA was induced by treating at the specified intervals with 2 µg/ml DOX. The cells were fixed and permeabilised in 3.7% PFA & methanol/EGTA. Centrosomes were labelled with γ-Tubulin (green) and β-catenin (red) and counterstained with DAPI. -CA cells show well-formed β-catenin at the apical region contrary to the disrupted and mislocalised β-catenin displayed by +CA cells. Scale bar 20µm. (C) The bar graph represents % CA in the population after the third DOX pulse (day 45) for 48 h. Error bars represent mean ± SEM from three biological repeats. (D) TEM image of 47-day MCF10A PLK4WT cell culture showing multi-layered vs bilayer formation with altered intercellular space in response to CA induction. Scale bar 4µm. (E) XY and Z-stack projections showing disruption of TJ protein ZO-1 (green) AJ protein β-catenin (red) at the apical region in CA+ conditions. The localisation of both ZO-1 & β-catenin were primarily in the apical region in both ± CA MCF10A PLK4 WT cells. Scale bar 20µm.

Figure 4: CA significantly disrupts and causes mislocalisation of tight junction and adherens junction proteins of the apical-lying MCF10A cells. (A) Representative confocal images of MCF10A cells stained for (left panels) AJ protein β-catenin (red) and TJ protein ZO-1 (green), and (right panels) TJ proteins JAM-A (red), occludin (green) showing localisation and intactness of epithelial cell junctions in ±CA MCF10A cells. CA was induced in 47-day cell culture model system using 2 µg/ml Dox. The cells were fixed and permeabilised in 3.7% PFA & 0.5% TritonX 100 respectively. The images are representative of three biological repeats. Scale bar 20µm. (B) Average grey value intensity values over 10 fields of view and (C) % cell junction disruption in 10 fields of view show that CA significantly altered the protein localisation and disrupted cell junctions respectively in +CA cells. The increased grey value intensity values of β-catenin and JAM-A indicated a change to brighter, more punctate localisation, whereas ZO-1 and Occludin showed an overall reduction in intensity of staining. Error bars represent mean ± sem from three independent experiments. Student T-test (Paired) was used for was used to determine the significance, ** $P \leq 0.01$, *** $P < 0.001$. (D) Representative images of (-CA) well-formed & (+CA) deformed tight junction (TJ), adherens junction (AJ) and desmosomes (DS) indicated by asterisk (*). The cells imaged at Mag=20000x, HV=100.0kV, Scale bar 600nm. (E) The bar graph represents the cell junction quantification showing a significant downregulation of adherens junctions (apical region) and a downward trend of tight junctions and desmosomes due to CA. Error bars represent mean ± sem from four independent experiments, and two-way ANOVA Bonferroni post-test was used to determine the significance, * $P < 0.05$.

Figure 5: Alteration of cytoskeletal structure and an increase autophagosome-like structure in + CA MCF10A cells. (A) Representative images of MCF10A PLK4 cells showing altered microfilaments structures in +CA cells. -CA cells show elongated filaments (indicated by arrows) compared to truncated, wavey filaments (indicated by arrows) in +CA cells. Cell junctions (AJ & DS) are indicated by an asterisk (*), Nu- nucleus. HV=100.0kV. Scale bar 200nm (white) and 600nm (black). (B) +CA cells show increased autophagosomes and phagophore-like structures near deformed cell junctions. Representative images of autophagosomes (arrow head) and phagophore-like structures (arrow) observed in + CA conditions. DS are indicated by asterisk (*). HV=100.0kV. Scale bar 500nm. (C) Quantification of autophagosomes observed in ±CA in 15 fields of view.

Figure 6: CA dysregulates tight junction formation in luminal breast cancer cell line MCF7 PLK4 WT. (A) Experimental layout of 10-day MCF7 PLK4 cell culture system. (B) Representative images of three biological repeats from ± CA MCF7 cells stained for (top panels) AJ protein β-catenin (red) TJ protein ZO-1 (green), (bottom panels) TJ proteins JAM A (red) and Occludin (green). CA was induced by treating cells with 2 µg/ml DOX for 48h. The cells were fixed and permeabilised in 3.7% PFA & 0.5% TritonX 100 respectively. Scale bar 20µm. (C) The bar graph represents quantification showing % cell junction disruption in MCF7 ± CA. n=2. (D) Representative images of MCF7 PLK4 cells showing normal tight junctions in -CA versus defective tight junctions in +CA (DS and TJ indicated by asterisk). Cells were fixed in primary fixative (2% glutaraldehyde + 2% paraformaldehyde + 0.1M sodium cacodylate) and secondary fixative (1% osmium tetroxide in 0.1M sodium cacodylate buffer pH 7.2) and imaged at Mag=20000x, HV=100.0kV, Scale bar 600nm. (E) The bar graph represents the cell junction quantification in TEM, with a decreasing trend in the tight junction formation in + CA MCF7 PLK4 cell lines. Error bars represent mean ± SEM from four independent experiments and a two-way ANOVA Bonferroni post-test was used to determine significance. $P > 0.05$.

Figure 7: CA dysregulates cell junction protein and cell adhesion molecule gene expression involved in breast cancer metastasis. (A) Western blot analysis shows representative images and graphs of quantification of fold-change in expression above β-actin/GAPDH controls across 3 independent experiments (±sem). CA dysregulates TJ proteins ZO-1, occludin and AJ protein β catenin total cell expression with no change in desmosome family total protein expression in +CA MCF10A PLK4 cells. CA was induced in MCF10A PLK4 cells cultured in -CT medium using 2 µg/ml Dox for 48h. Proteins were extracted at the indicated time point and quantified. (B) Representative images of subcellular fractionation Western blot analysis across 3 independent experimental repeats is shown. Altered recovery of the TJ proteins occludin and JAM-A in cytoskeletal fraction and redistribution of b-catenin and occludin to the nuclear fraction were all noted as effects of CA. (C) Of the 84 genes analysed, CA significantly upregulated MMP1, MMP13, ITGB3, FNI and downregulated MMP16, TIMP3 and PECAM1 gene expression. The final data represented in the table are from three independent experiments.

Lower limit of detection, the CT cut-off value-35. The p-values calculated by Student's t-test of the replicate 2^ (- Delta CT) values for each gene in the control group and treatment groups.

SUPPLEMENTAL FIGURE LEGENDS

Figure S1: **CA induced by CDK1 inhibition increases *in vitro* migration and invasion of MCF10A cells and blocking CA does not affect migratory or invasive capacity of TNBC cell line MDA-MB-468.** (A) Bar graph representing % CA post RO3306 treatment. CA was induced in WT MCF10A with 10 µM CDK1 inhibitor RO3306 treatment for the indicated time points. Error bars represent mean ± sem from 3 independent experiments in which a total of 200 cells were counted per time point. CDK1 inhibition-induced CA increases cellular (B) invasion and (C) migration in WT MCF10A. (D) Blocking CA using Centrinone B in TNBC MDA-MB-468 cells with low endogenous CA did not significantly affect migration and invasion.

Figure S2: CA induces early secondary tumour characteristics in chicken xenograft model (A) Representative images of excised ± CA MCF10A/matrigel graft on the chicken xenograft model. (B) + CA conditions caused multifocal moderate to marked reaction of the chick chorioallantoic membrane to the Matrigel in contrast to a zero to mild reaction seen in the -CA graft. (C) The CA+ sections (enlarged box) showed increased hyperplasia and inflammatory infiltrate and secondary tumour characteristics including vascular proliferation, haemorrhaging with accompanying central necrosis.

Figure S3: **Doxycycline treatment and overexpression of a truncated PLK4 608 variant has no effect on localisation of tight junction and adherens junction proteins.** Additional representative images 47-day long term cell cultures. (A and B) Immunofluorescence staining of MCF10A PLK4 ±CA shows combinations of AJ protein β-catenin (red), TJ protein ZO-1 (green), and TJ protein JAM-A (red), occludin (green). These images are representative of 4 independent biological repeats. Scale bar 20µm. (C) Representative images of 47-day long term cell cultures of MCF10A 608 ± Dox immunofluorescently stained for AJ protein β-catenin (red), TJ protein ZO-1 (green) and TJ protein JAM-A (red), occludin (green) (n=2). Scale bar 20µm. Doxycycline treatment of MCF10A 608 did not disrupt apical cell junction localisation or barrier integrity in MCF10A 608 47-day culture.

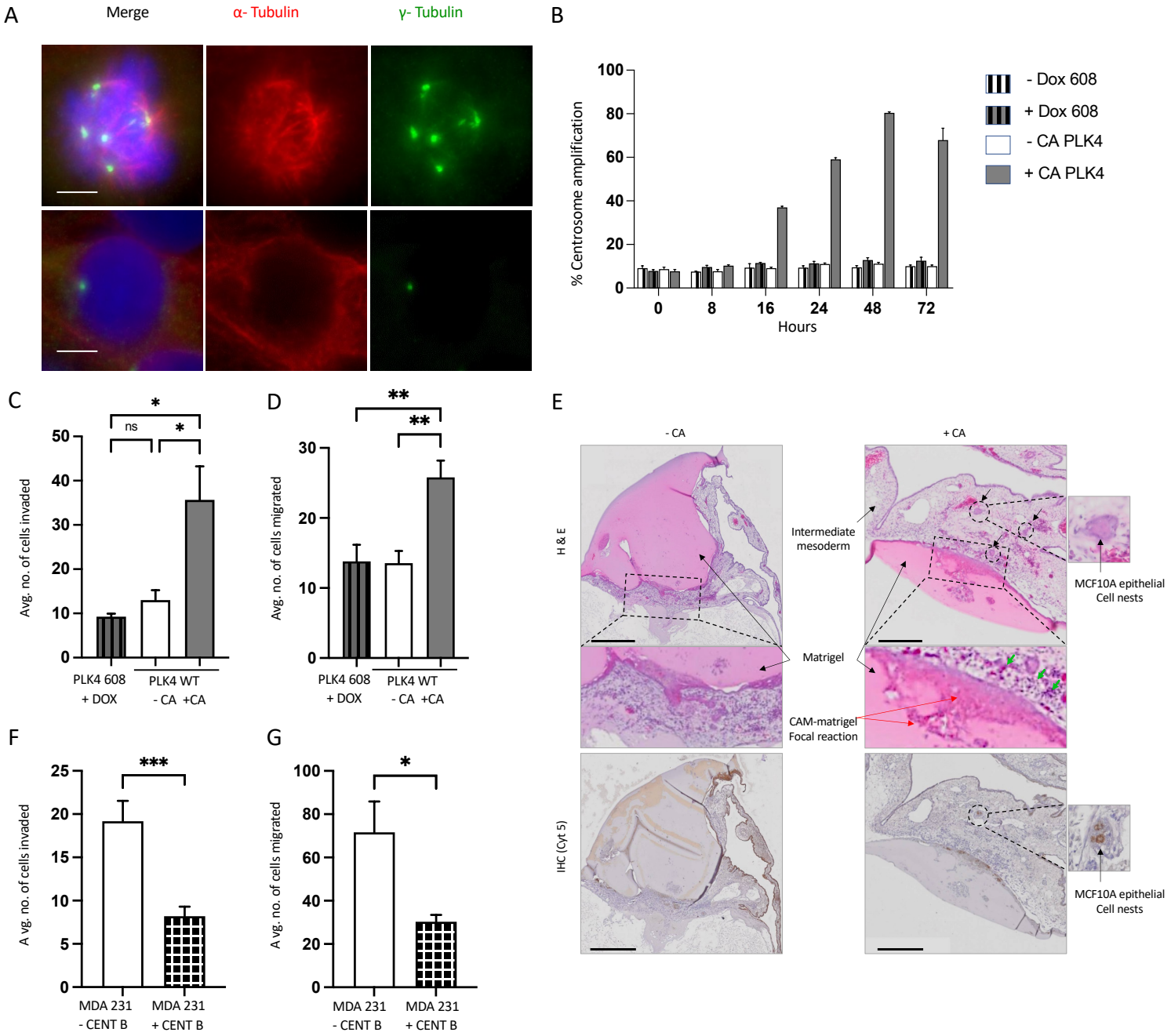
A
Merge
α- Tubulin
γ- Tubulin
B
% Centrosome amplification
100
80
60
40
20
0
0
8
16
24
48
72
Hours
- Dox 608
+ Dox 608
- CA PLK4
+ CA PLK4
C
Avg. no. of cells invaded
50
40
30
20
10
0
ns
*
*
PLK4 608
+ DOX
PLK4 WT
- CA +CA
D
Avg. no. of cells migrated
30
20
10
0
**
**
PLK4 608
+ DOX
PLK4 WT
- CA +CA
E
- CA
+ CA
H & E
Intermediate
mesoderm
MCF10A epithelial
Cell nests
Matrigel
CAM-matrigel
Focal reaction
IHC (Cyt 5)
MCF10A epithelial
Cell nests
F
A vg. no. of cells invaded
25
20
15
10
5
0
***
MDA 231
- CENT B
MDA 231
+ CENT B
G
A vg. no. of cells migrated
100
80
60
40
20
0
*
MDA 231
- CENT B
MDA 231
+ CENT B

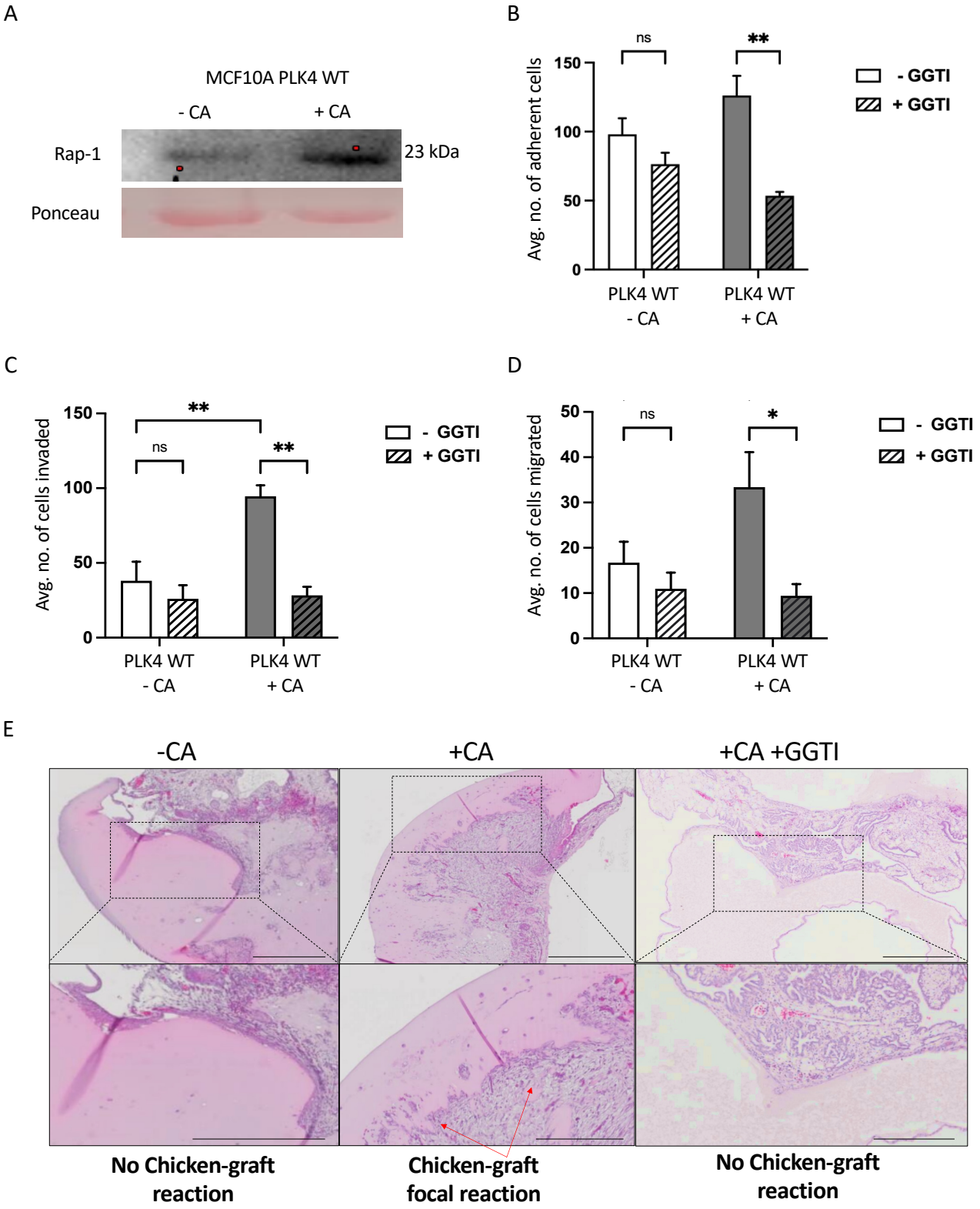
A
MCF10A PLK4 WT
- CA
+ CA
Rap-1
23 kDa
Ponceau
B
Avg. no. of adherent cells
150
100
50
0
ns
**
PLK4 WT - CA
PLK4 WT + CA
- GGTI
+ GGTI
C
Avg. no. of cells invaded
150
100
50
0
**
ns
**
PLK4 WT - CA
PLK4 WT + CA
- GGTI
+ GGTI
D
Avg. no. of cells migrated
50
40
30
20
10
0
ns
*
PLK4 WT - CA
PLK4 WT + CA
- GGTI
+ GGTI
E
-CA
+CA
+CA +GGTI
No Chicken-graft reaction
Chicken-graft focal reaction
No Chicken-graft reaction

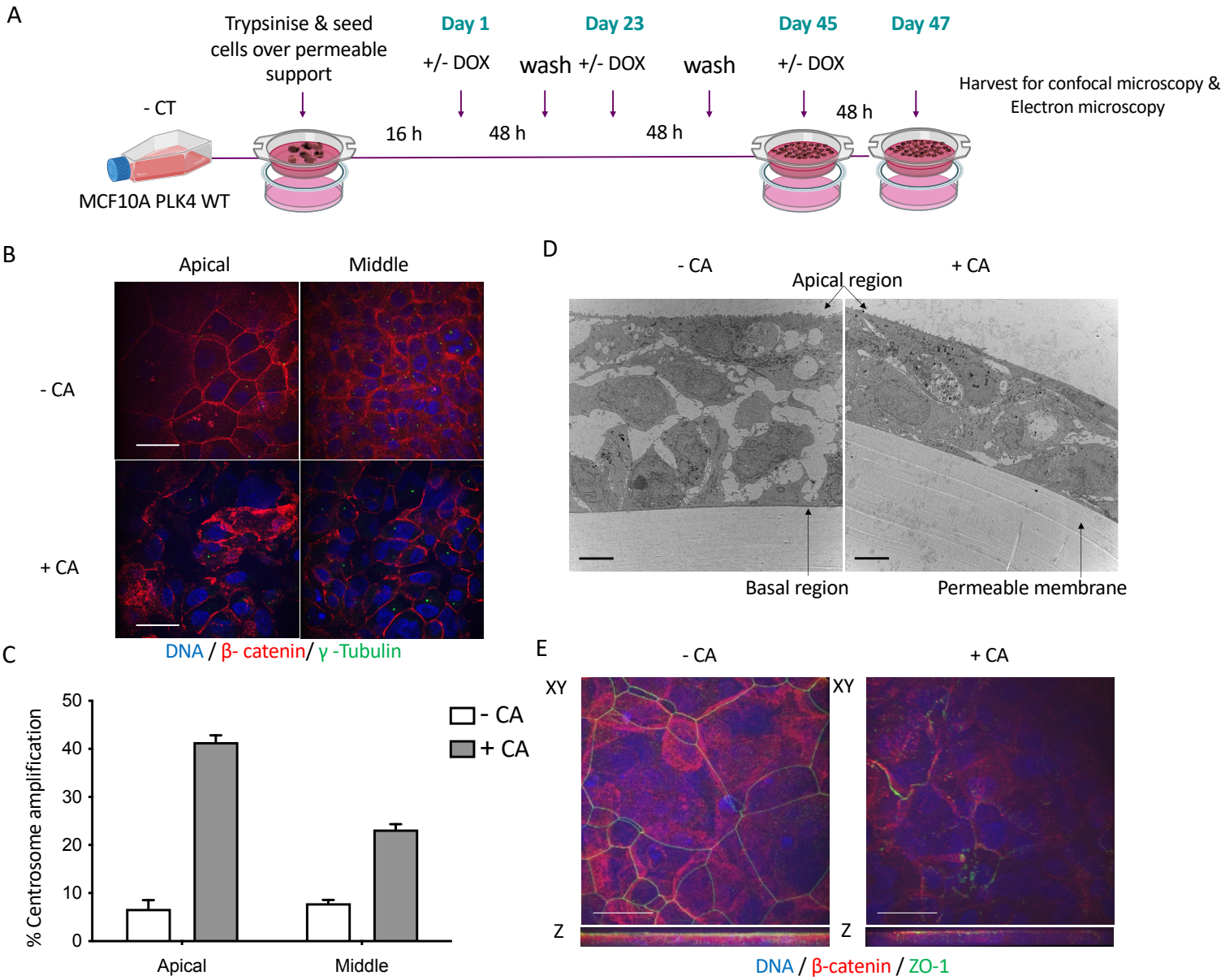
A
Trypsinise & seed cells over permeable support
Day 1
Day 23
Day 45
Day 47
+/- DOX
wash
+/- DOX
wash
+/- DOX
Harvest for confocal microscopy & Electron microscopy
- CT
16 h
48 h
48 h
48 h
MCF10A PLK4 WT
B
Apical
Middle
- CA
+ CA
DNA / β- catenin/ γ -Tubulin
C
% Centrosome amplification
50
40
30
20
10
0
- CA
+ CA
Apical
Middle
D
- CA
+ CA
Apical region
Basal region
Permeable membrane
E
- CA
+ CA
XY
XY
Z
Z
DNA / β-catenin / ZO-1

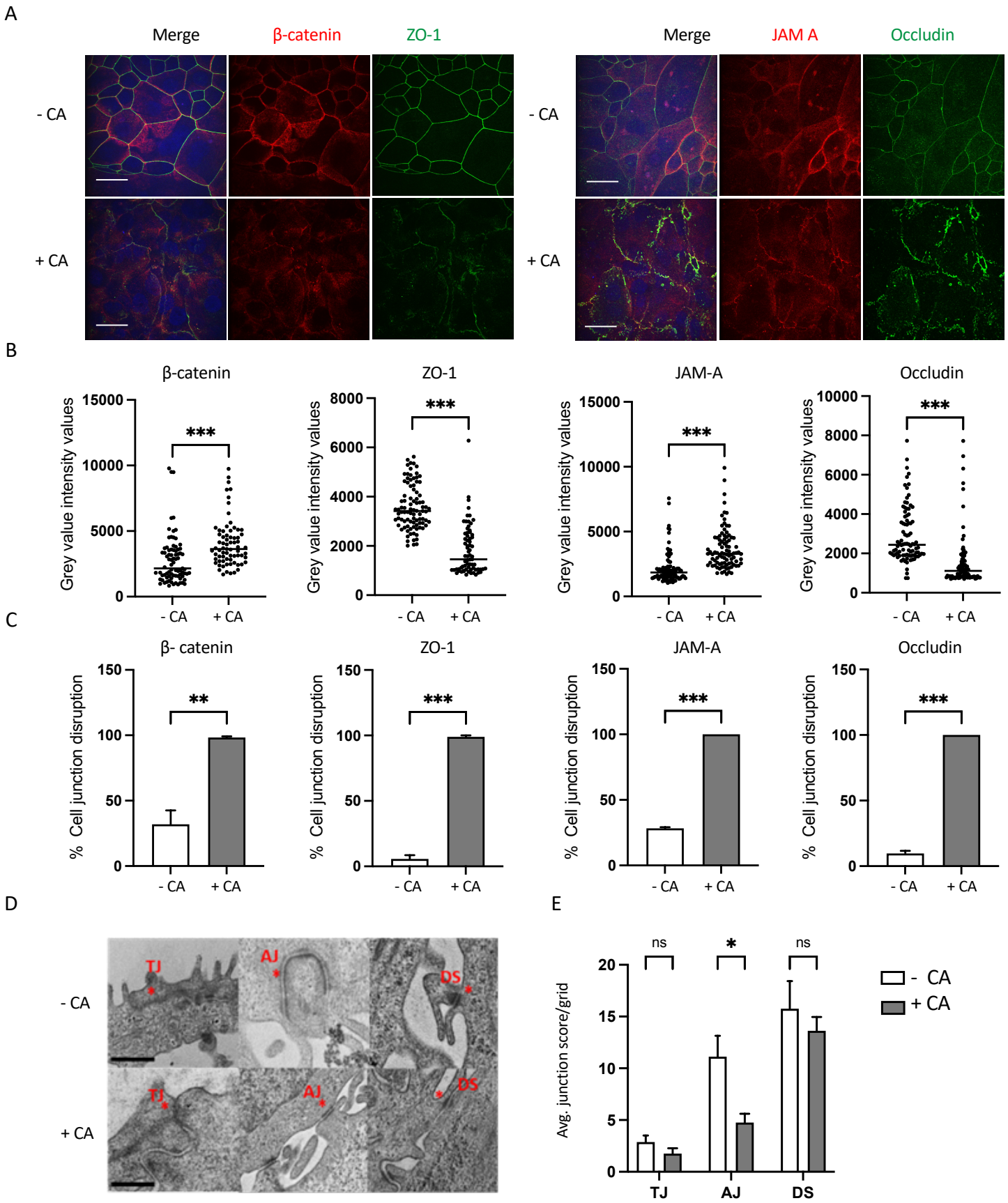
A
Merge
β-catenin
ZO-1
Merge
JAM A
Occludin
- CA
+ CA
B
β-catenin
ZO-1
JAM-A
Occludin
Grey value intensity values
***
- CA
+ CA
C
β- catenin
ZO-1
JAM-A
Occludin
% Cell junction disruption
**
***
D
TJ
AJ
DS
E
ns
*
Avg. junction score/grid
TJ
AJ
DS

FIGURE 5

Prakash et al, 2022

A

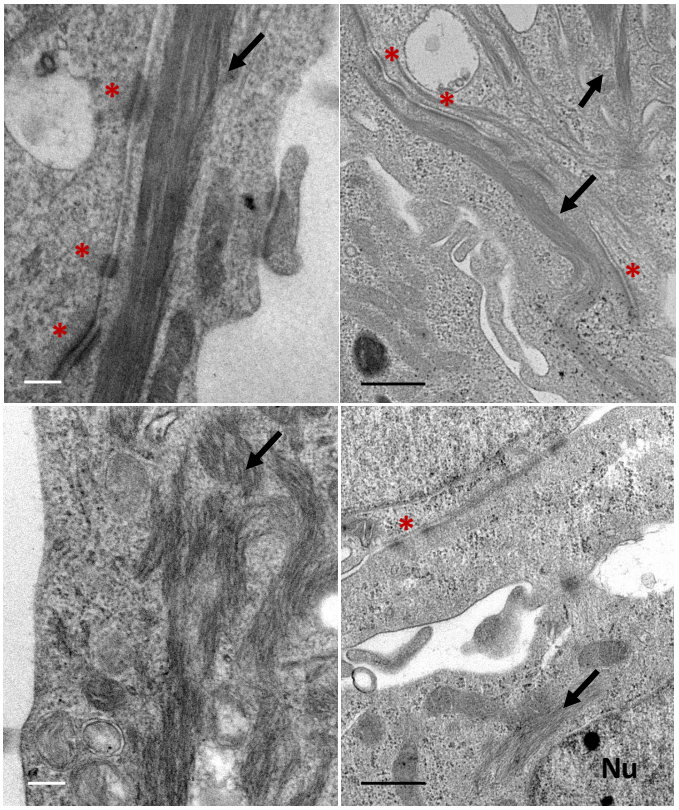

B

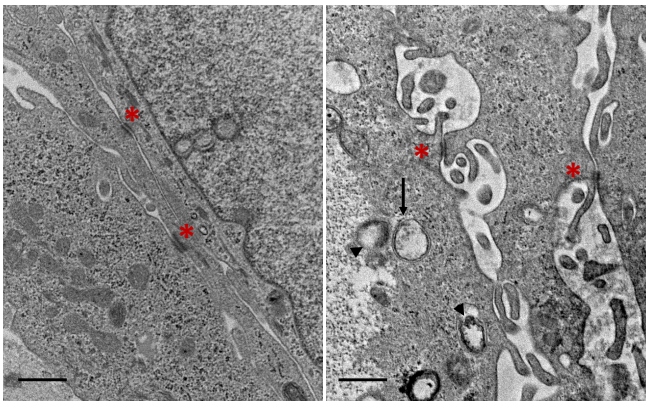

- CA + CA

C

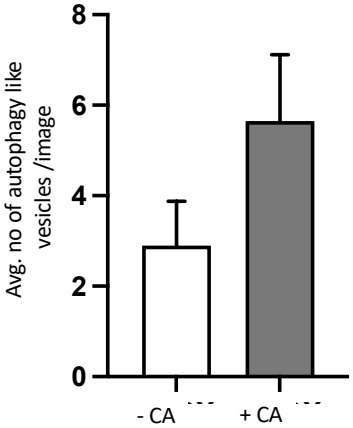

A

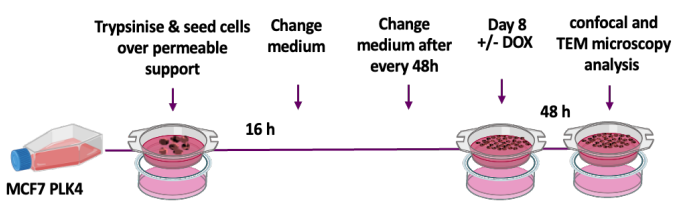
Trypsinise & seed cells over permeable support
Change medium
Change medium after every 48h
Day 8 +/- DOX
confocal and TEM microscopy analysis
16 h
48 h
MCF7 PLK4

B

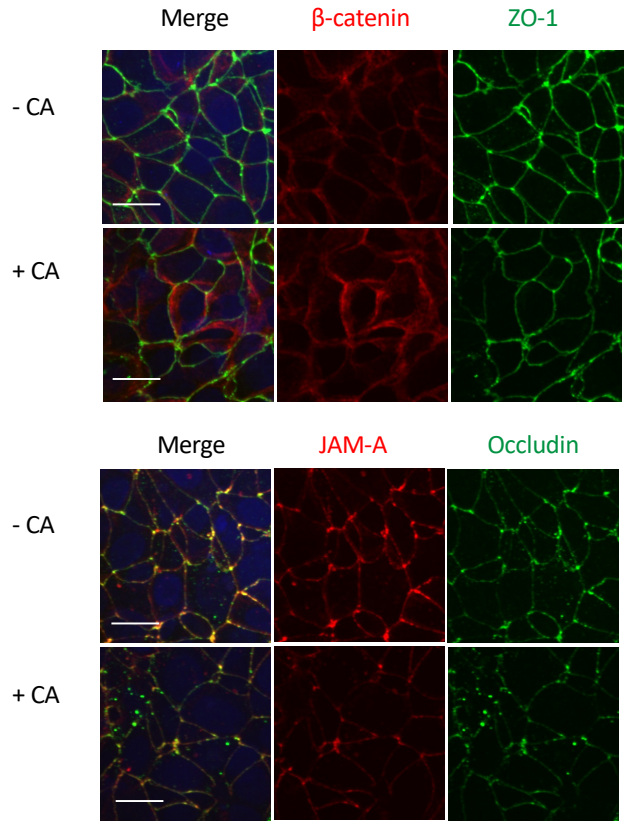
Merge
β-catenin
ZO-1
- CA
+ CA
Merge
JAM-A
Occludin
- CA
+ CA

C

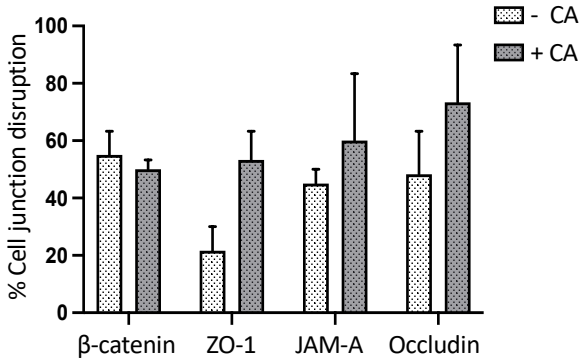
% Cell junction disruption
100
80
60
40
20
0
β-catenin
ZO-1
JAM-A
Occludin
- CA
+ CA

D

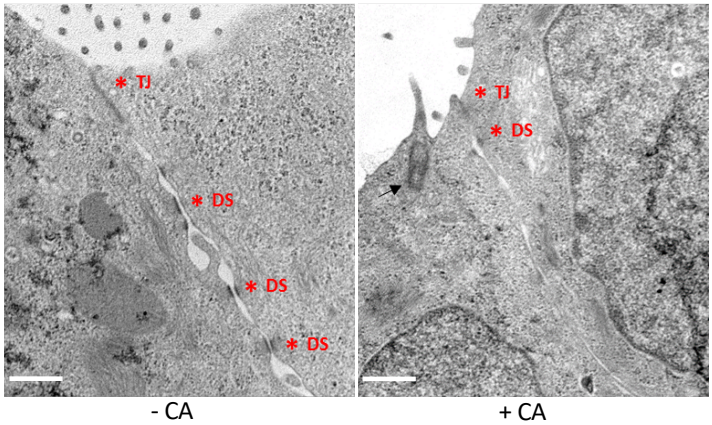
TJ
DS
DS
DS
TJ
DS
- CA
+ CA

E

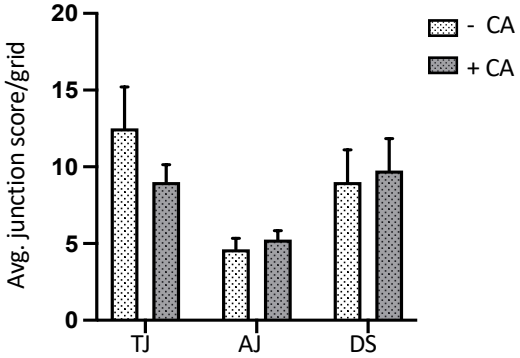
Avg. junction score/grid
20
15
10
5
0
TJ
AJ
DS
- CA
+ CA

A

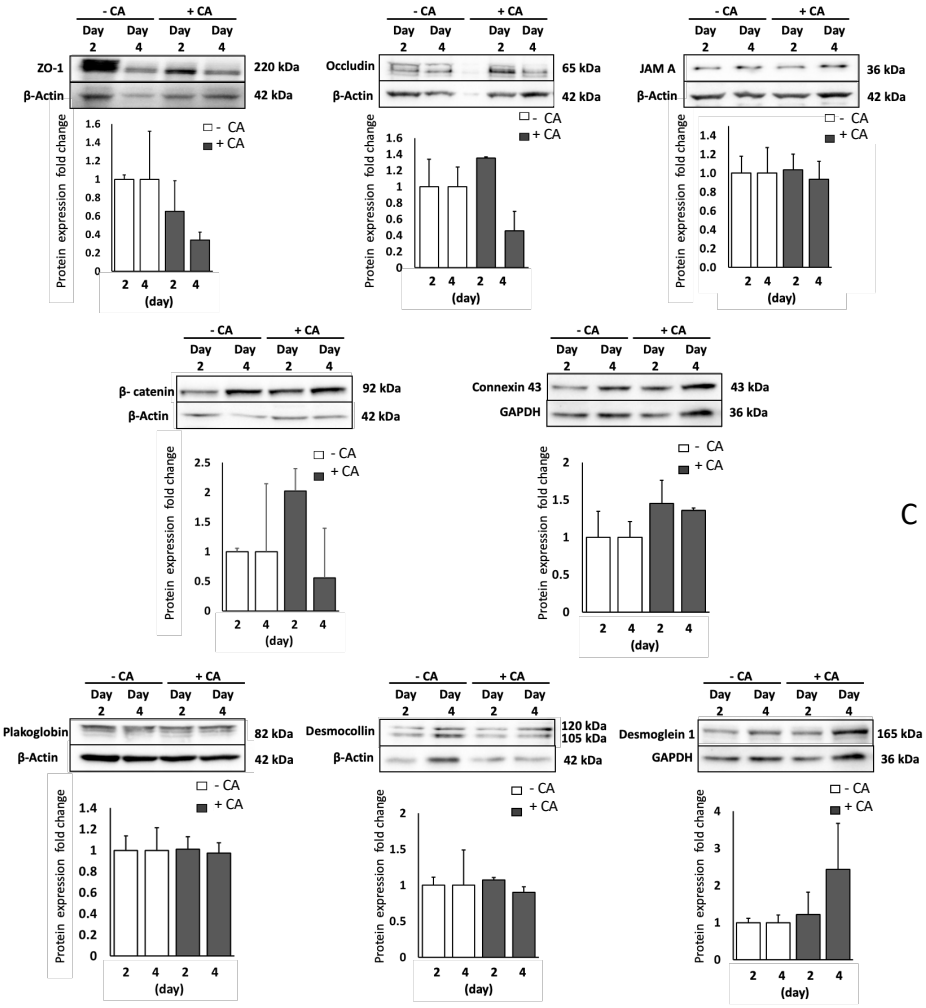

B

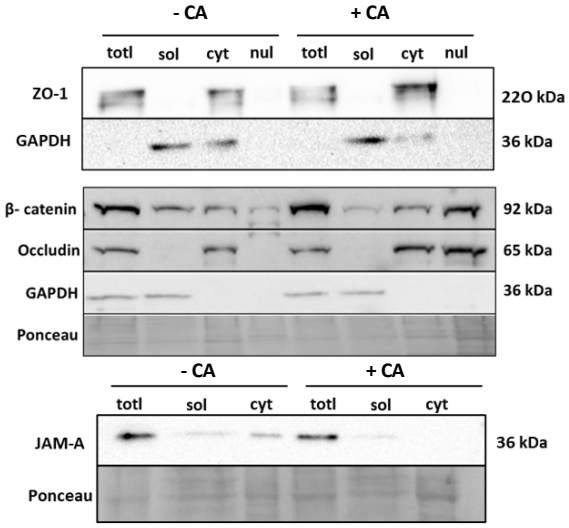

C

Genes significantly up-regulated as a result of CA in MCF10A PLK4^{WT} cells

Gene	Fold regulation	p-Value
MMPI	7.43	0.001525
ITGB3	2.96	0.035343
MMP13	2.09	0.048900
FN1	2.07	0.015939

Genes significantly down-regulated as a result of CA in MCF10A PLK4^{WT} cells

Gene	Fold regulation	p-Value
MMP16	-3.75	0.047223
TIMP3	-2.18	0.002895
PECAM1	-2.16	0.002369